VU VRIJE UNIVERSITEIT AMSTERDAM

VU Research Portal

Observation of molecular hyperfine structure in the extreme ultraviolet: The HF C-X spectrum

Philippson, J.N.; Shiell, R.C.; Reinhold, E.M.; Ubachs, W.M.G.

published in
Journal of Chemical Physics
2008

DOI (link to publisher)
10.1063/1.3006400

document version
Publisher's PDF, also known as Version of record

Link to publication in VU Research Portal

citation for published version (APA)
Philippson, J. N., Shiell, R. C., Reinhold, E. M., & Ubachs, W. M. G. (2008). Observation of molecular hyperfine structure in the extreme ultraviolet: The HF C-X spectrum. *Journal of Chemical Physics*, *129*(17), 174310. https://doi.org/10.1063/1.3006400

General rights
Copyright and moral rights for the publications made accessible in the public portal are retained by the authors and/or other copyright owners and it is a condition of accessing publications that users recognise and abide by the legal requirements associated with these rights.

- Users may download and print one copy of any publication from the public portal for the purpose of private study or research.
- You may not further distribute the material or use it for any profit-making activity or commercial gain
- You may freely distribute the URL identifying the publication in the public portal ?

Take down policy
If you believe that this document breaches copyright please contact us providing details, and we will remove access to the work immediately and investigate your claim.

E-mail address:
vuresearchportal.ub@vu.nl

Download date: 05. May. 2023

Observation of molecular hyperfine structure in the extreme ultraviolet: The HF *C*-*X* spectrum

Jeffrey N. Philippson,[1] Ralph C. Shiell,[1,a)] Elmar Reinhold,[2,b)] and Wim Ubachs[2]
[1]*Department of Physics and Astronomy, Trent University, Peterborough, Ontario K9J 7B8, Canada*
[2]*Laser Centre, Vrije Universiteit, De Boelelaan, 1081 HV Amsterdam, The Netherlands*

(Received 3 September 2008; accepted 6 October 2008; published online 7 November 2008)

Clearly resolved hyperfine structure has been observed in the extreme ultraviolet (XUV) spectra of the $C\ ^1\Pi$, $v=0-X\ ^1\Sigma^+$, $v=0$ transition of $H^{19}F$ obtained through 1 XUV+1 UV resonance enhanced multiphoton ionization spectroscopy. The hyperfine splitting within the *R*-branch lines shows significant perturbations, which we attribute to mixing with the rotational levels of the nearby $v=29$ level of the $B\ ^1\Sigma^+$ ion-pair state. A deperturbation analysis quantitatively explains the apparent variation of the fluorine magnetic hyperfine parameter a_F, for which a value of 4034(83) MHz was obtained by averaging over the values derived from the $R(0)-R(4)$ lines, after correcting for the effects of the perturbations. © *2008 American Institute of Physics*.
[DOI: 10.1063/1.3006400]

I. INTRODUCTION

For many reasons, hydrogen fluoride (HF) is one of the most intensely studied molecules, both experimentally[1,2] and theoretically.[3,4] In common with other hydrogen halides, HF provides a model system for studying molecular dissociation dynamics such as spin-orbit branching[5,6] and ion-pair formation.[7] Additionally, the large electronegativity of fluorine makes HF an interesting system for studying bond polarity,[8] and it is a well known gain medium within high power chemical lasers.[9]

Hyperfine resolved radio frequency spectra of the ground electronic state splitting due to nuclear spin-rotational and nuclear spin-spin interactions were observed using molecular beam magnetic and electric resonance as early as the 1960s.[10,11] Early analysis of the electronic spectrum of HF, including identification of the $C\ ^1\Pi$ state and interactions between the *e*-parity levels with the corresponding levels in the $B\ ^1\Sigma^+$ state, was undertaken by Douglas and Greening.[12] Hitchcock *et al.*[13] performed a detailed experimental and theoretical study of the electronic spectrum, determining absolute cross sections for several bands, and provided a useful overview of previous works. Tashiro *et al.*[14] used 1 XUV+1 UV (here XUV indicates extreme ultraviolet light, with wavelengths below the LiF cutoff) resonance enhanced multiphoton ionization (REMPI) spectroscopy. The linewidth ranged from 10 to 45 GHz permitting the $C\ ^1\Pi$ levels to be observed with rotational resolution.

Due to the large state densities in this highly excited energy region, interstate perturbations are both significant and numerous[15] and are expected to have strong rotational state dependence. Such perturbations can influence observed hyperfine structure by introducing additional hyperfine splitting into those eigenstates that, to first order, would have no splitting, and concomitantly reducing the observed splitting within other states. A quantitative analysis of this mixing can provide additional insight into the extent of the intramolecular interactions present in this highly excited energy region, one that has historically proven to be challenging both to access and understand.

The work presented herein represents a high-resolution extension of the experiment by Tashiro *et al.*[14] A linewidth of ~550 MHz has allowed us to directly observe hyperfine structure in the *C*-Rydberg state. Hyperfine resolved spectra of atomic Rydberg states have previously been observed in the VUV (Ref. 16) and XUV,[17] while hyperfine structure within molecular Rydberg states has been probed through millimeter-wave spectroscopy following initial excitation in the VUV.[18] To our knowledge, the work presented here is the first example of clearly resolved molecular hyperfine structure in Rydberg states observed through purely optical techniques.

II. THEORY

A. Magnetic hyperfine structure

The presence of nonzero nuclear spin in molecules can split spectral lines into numerous hyperfine components, with energy separations typically orders of magnitude smaller than those associated with the fine structure. The leading terms in the hyperfine Hamiltonian of an isolated molecule represent the energy of each nuclear magnetic dipole moment in the magnetic field due to the electrons, and each nuclear electric quadrupole moment in the electric field gradient. A nucleus with total angular momentum quantum number $I \leq 1/2$ has no electric quadrupole moment,[19] and therefore the $H^{19}F$ molecule, with two nuclei of spin $I_F=I_H=1/2$, has no such term in its hyperfine Hamiltonian.

The magnetic dipole hyperfine Hamiltonian includes a summation over the angular momenta of all electrons and nuclei. By projecting this operator onto the subspace of

a)Electronic mail: ralphshiell@trentu.ca.
b)Present address: National Institute for Subatomic Physics, Kruislaan 409, 1098 SJ Amsterdam, The Netherlands.

 © 2008 American Institute of Physics

Downloaded 30 Mar 2011 to 130.37.129.78. Redistribution subject to AIP license or copyright; see http://jcp.aip.org/about/rights_and_permissions

states within a given vibronic level, an effective Hamiltonian is obtained with terms that depend on either the total electronic orbital angular momentum **L** or the total electronic spin angular momentum **S**.[20] Particular details of the electronic spatial and spin distributions of the chemically important electrons in unfilled subshells can then be obtained from the resulting hyperfine parameters, providing a stringent test of high level theoretical calculations.

The ground state electronic configuration of HF is $1\sigma^2 2\sigma^2 3\sigma^2 1\pi^4$, giving rise to a $^1\Sigma^+$ term. The $C\ ^1\Pi$ state derives from the $1\sigma^2 2\sigma^2 3\sigma^2 1\pi^3 4\sigma$ electronic configuration, where the 1π and 4σ nonbonding orbitals are composed almost entirely of the fluorine $2p_{x,y}$ and $3s$ orbitals, respectively, at the ground state equilibrium geometry.[21] Because the unpaired 1π electron is the only electron to contribute to the time-averaged magnetic field experienced by each nucleus and, in the absence of an external field, this is localized near the fluorine nucleus, the hyperfine energy shift is expected to be dominated by the fluorine hyperfine term. The order in which the nuclear spins are coupled reflects this hierarchy.

The coupling scheme typically used for a molecule with two nonzero nuclear spins is a direct extension of Hund's case (a_β).[22] In case (a_β), **L** is strongly coupled to the internuclear axis by electrostatic forces and **S** is coupled less strongly by the spin-orbit interaction. The resulting vector **Ω** is then coupled to the molecular rotation to form **J**, which is subsequently coupled to the nuclear spin **I** to form the total angular momentum **F**. For the case of $H^{19}F$,

$$\mathbf{F}_1 = \mathbf{J} + \mathbf{I}_F, \tag{1}$$

$$\mathbf{F} = \mathbf{F}_1 + \mathbf{I}_H. \tag{2}$$

The basis kets under this coupling scheme can be expressed in the form $|\gamma\Lambda S\Sigma J I_F F_1 I_H F M_F\rangle$, where γ represents the electronic configuration and all other quantum labels required to uniquely define each state.

The general theoretical treatment of magnetic hyperfine structure in diatomic molecules is due originally to Frosch and Foley,[23] corrected slightly by Dousmanis,[24] and for states of well-defined Λ is now commonly partitioned into four terms representing distinct interactions. The effective Hamiltonian for a molecule with a single nuclear spin is given by

$$\hat{H}_{\rm hfs} = \hat{a}\hat{\mathbf{I}}\cdot\hat{\mathbf{L}} + \hat{b}_F\hat{\mathbf{I}}\cdot\hat{\mathbf{S}} + \hat{c}\left\{\hat{I}_z\hat{S}_z - \tfrac{1}{3}\hat{\mathbf{I}}\cdot\hat{\mathbf{S}}\right\} + \tfrac{1}{2}\hat{d}\{e^{2i\phi}\hat{I}^-\hat{S}^- + e^{-2i\phi}\hat{I}^+\hat{S}^+\}, \tag{3}$$

where the carets explicitly denote operators. For a $H^{19}F$ molecule in the $C\ ^1\Pi$ state, the effective magnetic hyperfine Hamiltonian takes the form

$$\hat{H}_{\rm hfs} = \hat{a}_F\hat{\mathbf{I}}_F\cdot\hat{\mathbf{L}} + \hat{a}_H\hat{\mathbf{I}}_H\cdot\hat{\mathbf{L}}. \tag{4}$$

For each nucleus, $\hat{a}$ is given, in SI units, by the expression[25]

$$\hat{a} = 2g_I\mu_N\mu_B\frac{\mu_0}{4\pi}\frac{1}{\Lambda}\sum_i\frac{\hat{l}_{z_i}}{r_i^3}. \tag{5}$$

Here, g_I is the respective nuclear g-factor, μ_N is the nuclear magneton, μ_B is the Bohr magneton, $\hat{l}_{z_i}$ is the projection on the internuclear axis of the orbital angular momentum of the ith electron, which is independent of the nucleus about which the orbital angular momentum is considered, and r_i is the magnitude of the position vector from the relevant nucleus to the ith unpaired electron. The factor of $\hat{l}_{z_i}/\Lambda$ within Eq. (5) represents the projection operator $\hat{\Phi}_i$ for a Hund's case (a) molecule, which projects the orbital angular momentum $\mathbf{l}_i$ of the ith electron onto the total electronic orbital angular momentum **L**.

For the $C\ ^1\Pi$ state of $H^{19}F$, in the absence of configuration mixing, the only electron for which l_{z_i} is nonzero is the single unpaired 1π electron and therefore the expression for $\hat{a}$ reduces to

$$\hat{a} = 2g_I\mu_N\mu_B\frac{\mu_0}{4\pi}\frac{1}{r^3}, \tag{6}$$

where r refers to this single electron and the two orbitals within the 1π subshell are the $2p_{x,y}$ orbitals of atomic fluorine. The diagonal matrix elements of each term in Eq. (4), for a state ψ, are proportional to the respective hyperfine parameter for each nucleus, $a=\langle\psi|\hat{a}|\psi\rangle$. These hyperfine parameters reflect the strength of the interaction between each nuclear spin and the electronic orbital angular momentum. Because they are proportional to $\langle\Sigma_i\hat{l}_{z_i}/r_i^3\rangle$, they also contain information about the spatial distribution of unpaired electrons within the molecule.

The hyperfine splitting of the ground electronic state ($\approx$300 kHz) (Ref. 11) is negligible compared to both that of the C-state and the experimental resolution we observe, and this was therefore neglected in the following analysis.

B. Λ-doubling

The hyperfine parameter a takes the same value for all rotational levels within a given *pure* vibronic state, however, for a $^1\Pi$-state rotational coupling can lead to mixing of the rotational levels of this degenerate electronic state with the corresponding levels of a Σ-state. All of the levels of a given Σ-state have the same e/f-parity, and each interacts with states of the same J and parity quantum number in the Λ-doublet, leading to splitting known as Λ-doubling. For interaction of a $^1\Pi$-state with *distant* $^1\Sigma$-states, this splitting is given by $qJ(J+1)$, where q is a Λ-doubling parameter, given by

$$q = 4\sum_{v,\Lambda}(-1)^s\frac{|\langle^1\Pi v'J|B(R)T^1_{+1}(\mathbf{L})|^1\Lambda^{\pm}vJ\rangle|^2}{E_{v'}-E_v}, \tag{7}$$

where the sum over Λ is taken over the Σ-states only, s is an integer that is even for Σ^+-states and odd for Σ^--states, and $B(R)$ is the usual rotational constant at internuclear distance R.

Downloaded 30 Mar 2011 to 130.37.129.78. Redistribution subject to AIP license or copyright; see http://jcp.aip.org/about/rights_and_permissions

If two states are energetically close, as is often the case for Rydberg states, the precise mixing between rotational states depends critically on their separation. In the case of the $C\ ^1\Pi$, $v=0$ state in HF, the *e*-parity component of the low-J levels mixes predominantly with the corresponding rotational level in the nearby $v=29$ vibrational level of the $B\ ^1\Sigma^+$ state.[14] These *e*-parity levels are probed in the *R*-branch *C-X* lines, while *Q*-branch lines probe the *f*-parity levels that do not interact with the *B*-state. Due to this mixing, we write the energy eigenstate labeled with quantum number J as

$$|J\rangle = c_1^J|C\ ^1\Pi, v=0, J\rangle + c_2^J|B\ ^1\Sigma^+, v=29, J\rangle. \tag{8}$$

The projection of this eigenstate onto the $|C\ ^1\Pi, v=0, J\rangle$ state determines the *mixing fraction*

$$\zeta_J \equiv |\langle C\ ^1\Pi, v=0, J|J\rangle|^2 = |c_1^J|^2. \tag{9}$$

An effect of this mixing is to introduce hyperfine splitting into those eigenstates that, to first order, derive from the $B\ ^1\Sigma^+$-state (and therefore are expected to have negligible hyperfine splitting), and also to reduce the splitting of those states consisting primarily of the $C\ ^1\Pi$-state. See Sec. IV for the calculation of these the mixing coefficients and their effects on the observed hyperfine structure.

III. EXPERIMENTAL DETAILS

The setup of the tunable narrowband XUV radiation source, including its application in high-resolution molecular spectroscopy studies, was described previously.[26] In short, the output of a continuous-wave ring-dye laser operating near 570 nm is amplified in a three-stage pulsed-dye amplifier (PDA), then frequency-doubled in a KDP nonlinear crystal and subsequently frequency tripled in a pulsed jet of xenon gas. Coherent radiation, tunable in the wavelength range near 95 nm is produced in a forwardly directed beam at sub-nanojoule pulse energies and at a bandwidth of 250–350 MHz, depending on specific alignment and conditions. This beam is perpendicularly crossed with a molecular beam of HF obtained from a pulsed solenoid valve (General Valve Series 9) and skimmed with a 1 mm diameter orifice. Signal is detected by resonant excitation of lines in the *C-X* (0,0) band and subsequent ionization by the UV laser beam that spatially and temporally overlaps the XUV beam. The 1 XUV+1 UV photoionization process produces HF^+ ions that are detected after pulsed field extraction and time-of-flight mass separation on a particle detector.

In contrast to the earlier experiment,[14] no absolute frequency measurements were performed in the present work. Relative frequency measurements are performed by comparing the XUV spectrum with the transmission markers of an actively stabilized etalon, for which the visible output of the ring-dye laser at the fundamental wavelength is used. While in absolute measurements the accuracy of the frequency scale is limited by chirp effect in the PDA system,[26] for the present relative measurements, the uncertainty is reduced to a few megahertz as the chirp effect is considered to be equal over the small frequency intervals of the scans. Hence the uncertainty in the derived hyperfine parameters is primarily due to the statistics of the fitting procedures.

IV. RESULTS AND ANALYSIS

A. Determination of the a_F hyperfine parameter

Each hyperfine-resolved rovibronic line was fitted individually to a simulated spectrum comprising the allowed hyperfine transitions, with the splitting of the upper state rotational level calculated using the Hamiltonian in Eq. (4). The laser system has a primarily Lorentzian profile and the simulated spectra were fitted accordingly, with the full width at half maximum linewidth $\Delta\nu$ treated as a free parameter in the fit. For the coupling case described above, the allowed electric dipole transitions within each line are given by $\Delta F=0,\ \pm 1\ (F=0\nrightarrow F'=0)$, $\Delta F_1=0,\ \pm 1\ (F_1=0\nrightarrow F_1'=0)$, and $\Delta M_F=0,\ \pm 1$.

The upper state energy splittings were obtained using first-order perturbation theory, resulting in values differing by <5 MHz compared with a full diagonalization approach, and this proved to be much less than the uncertainties in the fitted values of a_F.

For each line, the fitted values of a_F and $\Delta\nu$ were varied to minimize the sum of the squared errors between the experimental and simulated spectra. As discussed in Sec. II A, the hyperfine splitting due to the hydrogen nuclear spin was not clearly resolved, making it impossible to obtain the value of a_H from the fits. This splitting is expected to be small and within this experiment will contribute mainly to a broadening of the observed peaks with negligible effect on the derived value of a_F. A value of 107 MHz was used for the unperturbed value of a_H, predicted by theoretical calculations for the $X\ ^2\Pi$ state of HF^+.[25] Changes in the distributions of the core electrons are expected to decrease as the ionic limit is approached, and therefore the value for the ionic ground state should closely approximate that for the *C*-Rydberg state. The mixing fraction between the *C* and *B* states for each J was obtained from a deperturbation analysis, as described in Sec. IV B, and multiplied by the unperturbed value of a_H to provide an effective a_H in order to fit each *R*-branch line.

The matrix elements of Eq. (4) that correspond to the hyperfine energies associated with the F and H nuclei are labeled ME_F and ME_H, respectively,

$$\begin{aligned} ME_F = {} & \delta_{M_F M_F'}\delta_{FF'}\delta_{F_1F_1'}a_F\Lambda(-1)^{F_1+I_F+J+J'-\Lambda} \\ & \times\sqrt{(2J'+1)(2J+1)(2I_F+1)(I_F+1)I_F} \\ & \times\begin{Bmatrix} J' & I_F & F_1 \\ I_F & J & 1 \end{Bmatrix}\begin{pmatrix} J' & 1 & J \\ -\Lambda & 0 & \Lambda \end{pmatrix}, \end{aligned} \tag{10}$$

$$\begin{aligned} ME_H = {} & \delta_{M_F M_F'}\delta_{FF'}a_H\Lambda(-1)^{F+2F_1+I_H+2J'+I_F+1-\Lambda} \\ & \times\sqrt{(2J'+1)(2J+1)(2F_1'+1)(2F_1+1)} \\ & \times\sqrt{(2I_H+1)(I_H+1)I_H}\begin{Bmatrix} F_1' & I_H & F \\ I_H & F_1 & 1 \end{Bmatrix} \\ & \times\begin{Bmatrix} J' & F_1' & I_F \\ F_1 & J & 1 \end{Bmatrix}\begin{pmatrix} J' & 1 & J \\ -\Lambda & 0 & \Lambda \end{pmatrix}. \end{aligned} \tag{11}$$

Downloaded 30 Mar 2011 to 130.37.129.78. Redistribution subject to AIP license or copyright; see http://jcp.aip.org/about/rights_and_permissions

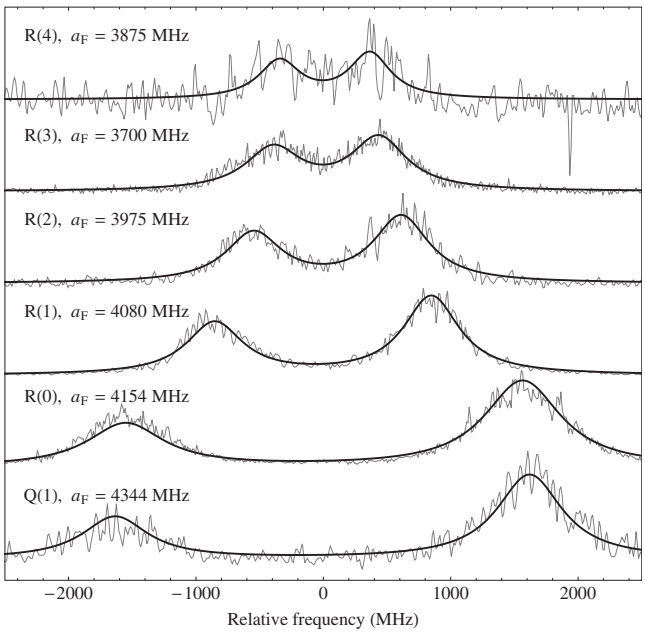

FIG. 1. REMPI spectra of the *C-X* transition in $H^{19}F$, with simulated spectra obtained using the matrix elements of the effective Hamiltonian given in Eqs. (10) and (11), with fitted a_F parameters as shown. The heights of the spectra have been rescaled for clarity.

The relative intensity S of each transition within a line, for linearly polarized incident light and the quantization axis parallel with the electric field, is given by

$$S = (2F+1)(2F'+1)(2F_1+1)(2F_1'+1) \times \begin{Bmatrix} F' & F_1' & I_H \\ F_1 & F & 1 \end{Bmatrix} \begin{Bmatrix} F_1' & J' & I_F \\ J & F_1 & 1 \end{Bmatrix} \times \left| \sum_{M_F=-F}^{F} \sum_{q=-1}^{1} \begin{pmatrix} F' & 1 & F \\ -M_F & 0 & M_F \end{pmatrix} \begin{pmatrix} J' & 1 & J \\ -\Lambda' & q & \Lambda \end{pmatrix} \right|^2 . \quad (12)$$

Little is known about the photoionization cross sections from the $C\ ^1\Pi$ state, but these are not likely to depend acutely upon the precise characteristics of each hyperfine level within a given rotational line, and therefore weighting with the one-photon linestrength S was deemed to be sufficient to describe the relative intensities of the total, two-photon transitions within each line.

The experimental and simulated spectra are shown in Fig. 1, from which the experimental *C-X* lineshapes are seen to be in good agreement with the theory, with fitted a_F parameters as shown in the figure. The average value of $\Delta\nu$ from the fits was 550 MHz, which is consistent with results from the narrow bandwidth laser described in Sec. III, crossed with a molecular beam. Intensity fluctuations in the $R(0)$ spectrum and low signal to noise ratio in the $R(4)$ spectrum resulted in values of $\Delta\nu$ that are ~150 MHz different from the other lines, but the derived values of a_F are not significantly affected by this parameter.

TABLE I. Mixing fractions ζ_J as defined by Eq. (9).

J	Mixing fraction
1	0.999 81
2	0.999 14
3	0.995 88
4	0.918 07
5	0.978 73

B. Deperturbation and determination of the *B-C* mixing coefficients

To calculate the mixing between near degenerate vibrational levels of the C and B states, the effective Hamiltonian approach must be abandoned in favor of a more general Hamiltonian that can couple rotational levels of different electronic states. Off-diagonal matrix elements between $B\ ^1\Sigma^+$, $v=29$ and $C\ ^1\Pi$, $v=0$ take the form $\beta\sqrt{J(J+1)}$, where β was obtained by deperturbation of line positions from Ref. 14. The 2×2 matrix constructed for each value of J using the basis states in Eq. (8) was diagonalized to obtain the eigenenergies and the eigenvectors, from which the mixing fractions ζ_J were obtained. The values of the rotational constant $B_{\Lambda-v}$ used were $B_{B-29}=104.701$ GHz and $B_{C-0}=403.2022$ GHz, while the heterogeneous rotational perturbation parameter took the value $\beta=75.7336$ GHz. See Table I for the calculated mixing fractions. Figure 2 shows how the rotational levels of the C and B states are shifted by this perturbation.

V. DISCUSSION

We determined whether the heterogeneous mixing can explain the apparent dependence of a_F on J for the various

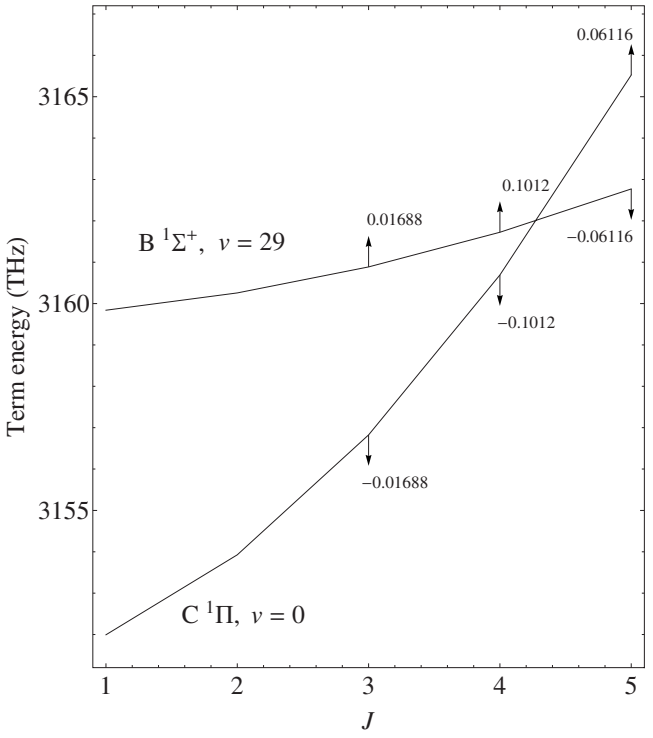

FIG. 2. The effects of perturbations between the rotational levels of the $B\ ^1\Sigma^+$, $v=29$ and $C\ ^1\Pi$, $v=0$ states of HF. The solid lines represent the energies of the unperturbed states, while the arrows show the energy shifts between perturbed (e-parity) and unperturbed (f-parity) states.

Downloaded 30 Mar 2011 to 130.37.129.78. Redistribution subject to AIP license or copyright; see http://jcp.aip.org/about/rights_and_permissions

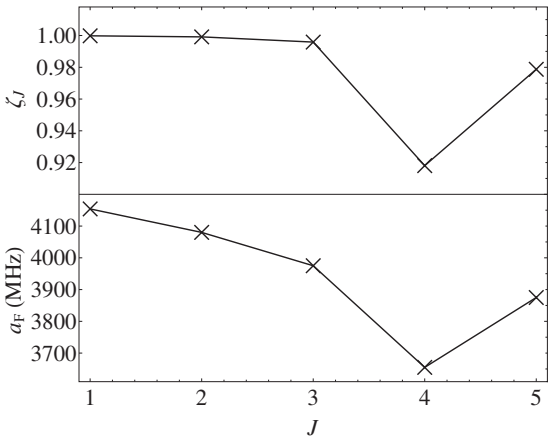

FIG. 3. (Upper panel) The mixing fraction ζ_J varies with the upper state J-value as shown. (Lower panel) The fitted value of a_F is seen to follow the same dependence with J.

R-branch transitions in the present study. From the selection rules for electric dipole transitions,[27] Q-branch transitions occur between states of different e/f-parity, while P- and R-branch transitions occur between states with the same parity. Consequently, the upper states of Q-branch C-X transitions in HF are the f-parity components of the Λ-doublets, which do not mix with the B-state. However, the upper states of the R-branch transitions are expected to have a fitted a_F that varies concomitantly with the mixing fraction ζ_J. Figure 3 shows how the values of a_F obtained from fitting the R-branch vary with the upper state J-value, and also the mixing fraction ζ_J.

Averaging over the fitted a_F values from the $R(0)-R(4)$ lines, after dividing each by its respective mixing fraction, resulted in a value for a_F of 4034(83) MHz. This result assumes that to the experimental precision achieved, the $B\ ^1\Sigma^+$, $v=29$ state is the only vibronic state to mix with the observed $C\ ^1\Pi$, $v=0$ levels. The fitted value of a_F from the $Q(1)$ line, for which there are no C-B perturbations, was found to be 4344 MHz, with an estimated uncertainty of ± 150 MHz, determined by comparing the simulated profile for different values of a_F with the extrema of the experimental profile envelope. These two values are in reasonable agreement. Any remaining difference may be due to the presence of other heterogeneous perturbations with states such as the $b\ ^3\Pi$ state discussed by Douglas and Greening.[12]

From Eq. (6), the hyperfine parameter a_F provides an experimental measurement of $\langle r^{-3}\rangle_{1\pi}$ with respect to the fluorine nucleus. It is interesting to compare this value for the C-state of HF with both that of $\langle r^{-3}\rangle_{1\pi}$ in HF^+, and also with $\langle r^{-3}\rangle_{2p}$ in F^+. The first indicates the degree of Rydberg character of the C-state, while the second indicates how similar the potential experienced by a 1π electron in the C-state, for which one electron has been removed from this subshell, is to that of the $2p$ orbital in a singly charged fluorine ion.

Two recent theoretical calculations and two experimental measurements of a_F in HF^+ have been published and these values, listed in Table II, are indeed similar to that which we observe in the C-state. Kristiansen and Veseth[25] used many-body perturbation theory to calculate a complete set of first-order magnetic hyperfine parameters, allowing a comparison of the electronic spatial and spin distributions because $a/(d+(1/3)c)=\langle r^{-3}\rangle_{\text{orb.}}/\langle r^{-3}\rangle_{\text{spin}}$. Bruna and Grein[28] used density functional methods to calculate a more restricted set of parameters, with the a-parameter obtained from c and d, assuming that $\langle r^{-3}\rangle_{\text{orb.}}=\langle r^{-3}\rangle_{\text{spin}}$. Coe *et al.*[29] used direct laser absorption spectroscopy in fast ion beams to obtain a complete set of experimentally derived magnetic hyperfine constants. Allen *et al.*[30] used far-infrared laser magnetic resonance spectroscopy to obtain the four magnetic hyperfine parameters.

TABLE II. The derived values of the a_F hyperfine parameter in HF and HF^+ from this and other works. Values for $\langle r^{-3}\rangle$, for the 1π and $2p$ orbitals in HF/HF^+ and F^+, respectively, are given for comparison as described in the text.

Species	Term	a_F [a]	$\langle r^{-3}\rangle$ [b]	Reference
HF	$C\ ^1\Pi$	4034(83)	54.31	tw[c]
HF^+	$X\ ^2\Pi$	3957.87	53.2430	25[d]
HF^+	$X\ ^2\Pi$	4164(15)[e]	56.02	28[d]
HF^+	$X\ ^2\Pi$	3850(31)	51.79	29[c]
HF^+	$X\ ^2\Pi$	3985.81	53.619	30[c]
F^+	^3P	—	56.7455	31[d]

[a]Values given in megahertz.
[b]Values given in $Å^{-3}$.
[c]Experimental. tw corresponds to this work, derived from the R-branch lines.
[d]Theoretical.
[e]Value of $\langle r^{-3}\rangle_{\text{orb.}}$ approximated by $\langle r^{-3}\rangle_{\text{spin}}$, equivalent to assuming $a=d+c/3$.

Our derived value of $\langle r^{-3}\rangle_{\text{orb.}}$ for the 1π orbital is also in reasonable agreement with the calculated corresponding value for the $2p$ orbital of F^+.[31] The value given in Table II is that derived using polarization wave functions that yield hyperfine parameters in better agreement with experiment than alternative choices of configuration interaction wave functions. The hyperfine structure within the ^3P ground state of F^+ was also studied experimentally by Brown *et al.*[32] using laser magnetic resonance spectroscopy. By combining their experimentally derived value for A_J with the calculated values of $\langle r^{-3}\rangle_{\text{spin.}}$ and $|\psi(0)|^2$ from Schaefer and Klemm,[31] broad agreement can be seen for the value of $\langle r^{-3}\rangle_{\text{orb.}}$. This indicates the validity of the assumed electron configuration of the C-state.

In summary, we have presented results from hyperfine-resolved REMPI spectra of the C-X transition in HF, observed through XUV REMPI spectroscopy with a linewidth of 550 MHz. The R-branch transitions show fitted fluorine magnetic hyperfine parameters that vary with J. A quantitative analysis of the rotational coupling between the B and C states has yielded mixing fractions and energy shifts, and largely explains the observed variation in the fitted value of a_F. The single value of a_F derived from these spectra is compared with that from a Q-branch line, which does not experience this perturbation.

ACKNOWLEDGMENTS

This study was supported by the European Community-Integrated Infrastructure Initiative action LASERLAB-

Downloaded 30 Mar 2011 to 130.37.129.78. Redistribution subject to AIP license or copyright; see http://jcp.aip.org/about/rights_and_permissions

Europe (RII3-CT-2003-506350) and NSERC (Canada). We wish to acknowledge John Brown for useful discussions. J.N.P. acknowledges Queen's University for financial support.

[1] E. Safary, J. Romand, and B. Vodar, J. Chem. Phys. **19**, 379 (1951).
[2] J. W. C. Johns and R. F. Barrows, Proc. R. Soc. London, Ser. A **251**, 504 (1959).
[3] C. F. Bender and E. R. Davidson, J. Chem. Phys. **47**, 360 (1967).
[4] P. E. Cade and W. M. Huo, J. Chem. Phys. **47**, 614 (1967).
[5] J. Zheng, C. W. Riehn, M. Dulligan, and C. Wittig, J. Chem. Phys. **104**, 7027 (1996).
[6] A. Brown and G. G. Balint–Kurti, J. Chem. Phys. **113**, 1870 (2000).
[7] Q. J. Hu and J. W. Hepburn, J. Chem. Phys. **124**, 074311 (2006).
[8] S. Raub and G. Jansen, Theor. Chem. Acc. **106**, 223 (2001).
[9] D. J. Spencer, T. A. Jacobs, H. Mirels, and R. W. F. Gross, Int. J. Chem. Kinet. **1**, 493 (1969).
[10] M. R. Baker, H. Mark Nelson, J. A. Leavitt, and N. F. Ramsey, Phys. Rev. **121**, 807 (1961).
[11] R. Weiss, Phys. Rev. **131**, 659 (1963).
[12] A. E. Douglas and F. R. Greening, Can. J. Phys. **57**, 1650 (1979).
[13] A. P. Hitchcock, G. R. J. Williams, C. E. Brion, and P. W. Langhoff, Chem. Phys. **88**, 65 (1984).
[14] L. M. Tashiro, W. Ubachs, and R. N. Zare, J. Mol. Spectrosc. **138**, 89 (1989).
[15] H. Lefebvre–Brion and R. W. Field, *The Spectra and Dynamics of Diatomic Molecules* (Academic, Orlando, 2004).
[16] H. J. Wörner, M. Grütter, E. Vliegen, and F. Merkt, Phys. Rev. A **71**, 052504 (2005).
[17] T. Trickl, M. J. J. Vrakking, E. Cromwell, Y. T. Lee, and A. H. Kung, Phys. Rev. A **39**, 2948 (1989).
[18] A. Osterwalder, A. Wuëst, F. Merkt, and Ch. Jungen, J. Chem. Phys. **121**, 11810 (2004).
[19] H. Enge, *Introduction to Nuclear Physics* (Addison Wesley, Reading, MA, 1966).
[20] J. Brown and A. Carrington, *Rotational Spectroscopy of Diatomic Molecules* (Cambridge University Press, Cambridge, 2003).
[21] R. K. Chaudhuri, K. F. Freed, S. A. Abrash, and D. M. Potts, J. Mol. Struct.: THEOCHEM **547**, 83 (2001).
[22] E. Hirota, *High Resolution Spectroscopy in Transient Molecules* (Springer-Verlag, Berlin, 1985).
[23] R. A. Frosch and H. M. Foley, Phys. Rev. **88**, 1337 (1952).
[24] G. C. Dousmanis, Phys. Rev. **97**, 967 (1955).
[25] P. Kristiansen and L. Veseth, J. Chem. Phys. **84**, 6336 (1986).
[26] W. Ubachs, K. S. E. Eikema, W. Hogervorst, and P. C. Cacciani, J. Opt. Soc. Am. B **14**, 2469 (1997).
[27] J. M. Brown, J. T. Hougen, K. P. Huber, J. W. C. Johns, I. Kopp, H. Lefebvre–Brion, A. J. Merer, D. A. Ramsay, J. Rostas, and R. N. Zare, J. Mol. Spectrosc. **55**, 500 (1975).
[28] P. J. Bruna and F. Grein, Mol. Phys. **104**, 429 (2006).
[29] J. V. Coe, J. C. Owrutsky, E. R. Keim, N. V. Agman, D. C. Hovde, and R. J. Saykally, J. Chem. Phys. **90**, 3893 (1989).
[30] M. D. Allen, K. M. Evanson, and J. M. Brown, J. Mol. Spectrosc. **227**, 13 (2004).
[31] H. F. Schaefer III and R. A. Klemm, Phys. Rev. A **1**, 1063 (1970).
[32] J. M. Brown, L. R. Zink, and K. M. Evanson, Phys. Rev. A **57**, 2507 (1998).

Downloaded 30 Mar 2011 to 130.37.129.78. Redistribution subject to AIP license or copyright; see http://jcp.aip.org/about/rights_and_permissions